

*A NEW
SHADOWGRAPHIC
METHOD OF VIEWING
RAYLEIGH-BENARD
CONVECTION IN A
CYLINDER OF LOW
ASPECT RATIO*

**WILLIAM J. O'BRIEN and
MATTHEW LEES**

May 1999

TABLE OF CONTENTS

1. INTRODUCTION.....	3
2. RAYLEIGH-BENARD CONVECTION.....	4
2.1 THE PRANDTL NUMBER.....	4
2.2 THE CRITICAL TEMPERATURE DIFFERENCE	5
2.3 THE OBERBECK-BOUSSINESQ EQUATIONS.....	7
2.3 THE BIFURCATION AT THE ONSET OF CONVECTION.....	8
2.3 STRAIGHT ROLL CONVECTION.....	11
2.6 THE EFFECTS OF THE SIDEWALLS.....	13
2.7 BUSSE BALLOONS AND TIME DEPENDENT FLOW	14
2.8 OTHER TIME-INDEPENDENT PATTERNS.....	15
3. SHADOWGRAPHY.....	16
3.1 SHADOWGRAPHY VS SCHLIEREN	18
3.2 THE TWO-LENS SYSTEM	18
3.3 THE FOUR-LENS SYSTEM	20
3.4 LENS SELECTION	22
4. EXPERIMENTATION.....	23
4.1 PREVIOUS EXPERIMENTS.....	23
4.2 EXPERIMENTATION WITH THE FOUR-LENS SYSTEM	23
4.3 A COMPARISON BETWEEN OPTICAL SYSTEMS.....	25
5. CONCLUSIONS	27

TABLE OF FIGURES

FIGURE 1.	TEMPERATURE PROFILE BETWEEN PLATES (AVERAGED OVER THE WIDTH) IN CONDUCTIVE AND CONVECTIVE REGIMES [1].	8
FIGURE 2	THE PSEUDO- POTENTIAL WITH ORDER PARAMETER v .	9
FIGURE 3.	THE VELOCITY AT ANY PARTICULAR POINT UNDERGOES A NORMAL BIFURCATION AT $R = R_{\text{CRIT}}$.	10
FIGURE 4.	AT THE ONSET OF CONVECTION, THE RISING SPHERE OF WARM FLUID (RED) MEETS A FALLING COOLER SPHERE, AND DOESN'T KNOW WHICH WAY TO MOVE.	10
FIGURE 5.	THE NUSSELT NUMBER SUDDENLY INCREASES FROM 1 AT THE ONSET OF CONVECTION.	11
FIGURE 6.	STRAIGHT ROLL CONVECTIVE MOTION.	12
FIGURE 7.	THE MARGINAL STABILITY CURVE, DIVIDING THE TWO MAIN REGIMES.	12
FIGURE 8.	CRITICAL RAYLEIGH NUMBERS FOR CYLINDRICAL CONVECTION CHAMBERS WITH INSULATING SIDEWALL, [10].	14
FIGURE 9.	A THREE-ROLL PATTERN IN A CYLINDRICAL CONTAINER OF SMALL ASPECT RATIO.	14
FIGURE 10.	THE BUSSE BALLOON FOR A FLUID WITH $Pr = 7$. [11].	16
FIGURE 11.	BUSSE BALLOON FOR AIR. $Pr = 0.7$ [11].	17
FIGURE 12.	THE ORIGINAL 'TWO' LENS CROQUETTE SYSTEM.	18
FIGURE 13.	THE CONVECTIVE CELL HAS AN OVERALL FOCAL LENGTH OR FOCALISATION DISTANCE F [5].	20
FIGURE 14.	THE FOUR-LENS SYSTEM LAYOUT, IN TERMS OF LENS FOCAL LENGTHS.	21
FIGURE 15.	DIAGRAM OF THE CONVECTION CELL.	21
FIGURE 16.	IMAGES OF THE NON-CONVECTING FLUID CELL, SHOWING THE MAIN UNWANTED REFLECTION.	22
FIGURE 17.	STABILITY REGIMES AND EVOLUTION OF THE BASIC PATTERNS FOUND BY BJORN HOF [12,13].	23
FIGURE 18.	TWO ROLL, MERCEDES AND FOUR ROLL PATTERN IMAGES TAKEN WITH THE FOUR-LENS SYSTEM.	24
FIGURE 19.	THE FOUR BASIC FLOW STATES AND THEIR INVERTED PATTERNS.	24

TABLE OF TABLES

TABLE 1 - PRANDTL NUMBERS [1, 4, 5, 6].		5
TABLE 2	SOME IMPORTANT PROPERTIES OF WATER [6, 7].	6
TABLE 3	CRITICAL TEMPERATURE DIFFERENCES [1, 4, 5].	6
TABLE 4	ΔT TO RAYLEIGH NUMBER CONVERSION.	7
TABLE 5.	DATA FOR THE FOUR MAIN LENSES IN OUR SYSTEM.	22
TABLE 6.	COMPARISON OF THE FRACTIONAL RESOLUTION OVER VARIOUS FLOW STATES FOR THE PENTAGON ROI.	26
TABLE 7.	COMPARISON OF THE FRACTIONAL RESOLUTION OVER VARIOUS FLOW STATES FOR STRIP ROI.	26
TABLE 8.	COMPARISON OF RECALCULATED RAYLEIGH NUMBERS.	28

1. INTRODUCTION

Convection is a form of heat transfer within a fluid that involves bulk motion within a gravitational field. Let us suppose that some fluid in a vertical container is warmer nearer the bottom than nearer the top. It seems reasonable to think that buoyancy forces will cause fluid at the bottom to move upwards towards the top. However this motion is subject to resistive forces. In the case of most fluids this is due to its viscosity. As a result it turns out that convection will only take place in this container if the temperature difference between the top and bottom exceeds a certain critical value. The subject of convection is of great importance to various aspects of scientific research. For example it is a very important method of heat transfer in weather systems and the other envelopes of stars. The granular structure in the Sun's photosphere is a result of convection. The production of pure semi-conductors involves convective processes [1].

Rayleigh-Bénard convection is an idealised convection situation in which the fluid is contained vertically between a pair of conducting plates held at constant temperatures. The fluid's motion is subject to what are called rigid-rigid boundary conditions, which arise from the fact the fluid cannot move through the plates. Water in an ocean, by contrast, is subject to rigid-free boundary conditions. There are many interesting ways in which the fluid can move between the two plates in Rayleigh-Bénard convection. The pattern that the fluid chooses depends not only on the current situation but also on the way in which that situation was reached. There are stable convection patterns, which keep roughly the same form over time, and there are unstable or turbulent patterns, which change with time. The most simply pattern obtainable is the straight-roll pattern, where the fluid forms long tubes of rotating fluid perpendicularly to the plates. In our experiment the chamber used was a cylindrical one with Perspex sidewalls and an aspect ratio (radius divided by height) of 2. The conducting plates were held at constant temperature using a water pump. This rather low aspect ratio has a fairly big influence on the fluid's properties and the patterns we see. With such a chamber it is possible to produce straight (or curved roll) patterns, spoked patterns, concentric ring patterns as well as time-dependent patterns.

Our method of observing the convection was to use shadowgraphy. The apparatus in the laboratory at the start of our experimentation was that used by Bjorn Hof in his MSc project. It employed two converging lenses and a CCD camera. Although this set up was capable of producing images of good contrast, they were small and didn't fill the CCD screen. We decided to try an alternative set-up with four lenses, which had been suggested by Vincent Croquette in [2]. He proposed that this set-up would widen the ray bundle to produce larger images without degrading the contrast.

In our experiment our first aim was to set up a four-lens observing system. Our second aim was to reproduce some of the convection patterns that were described in B. Hof's thesis and to compare images of those patterns with those obtained using the two-lens system, making quantitative measurements to check for contrast loss.

In section 2 of this article a brief discussion of Rayleigh-Bénard convection shall be given and the differences between chambers of infinite horizontal extent and chambers of finite horizontal extent in section 2. A detailed description of the apparatus used for producing shadowgraphic images shall be discussed in section 3. Descriptions and images of the patterns and the means by which they were produced shall be discussed in section 4.

2. RAYLEIGH-BENARD CONVECTION

2.1 The Prandtl number

All convecting fluids have two crucial parameters in determining their flow. One of these is its thermal diffusivity, which is given by the formula [3],

$$D_T = \frac{\kappa}{\rho C_p}$$

where κ is the thermal conductivity, C_p is the specific heat capacity at constant pressure and ρ is the density. It is a measure of how quickly phonons can diffuse through the fluid and dissipate their energy to the fluid's particles. The second is its kinematic viscosity, which is given by this formula,

$$\nu = \frac{\eta}{\rho}$$

where η is the dynamic viscosity. The ratio, ν / D_T , is a dimensionless quantity called the Prandtl number (Pr). A few Prandtl numbers are displayed in table 1.

TABLE 1 - PRANDTL NUMBERS [1, 4, 5, 6]

FLUID	P_r
Air	0.7
Liquid helium (2.3K, SVP)	0.57
Mercury	0.025
Water (10°C)	9.28
(20°C)	6.94
(30°C)	5.39
(40°C)	4.30
(50°C)	3.54
Carbon Dioxide (300K, 40bar)	1.46
Silicon oil	900

Fluids of similar Prandtl number have similar convective properties. We cannot obtain shadowgraphic images of liquid metals due to their opacity. The convective properties of liquid helium are at an midpoint between media such as air and liquid metals [3]. This gives us an incentive to study convection in liquid helium. It is unfortunately difficult to perform shadowgraphy with liquid helium because its refractive index is very close to 1 and changes little with temperature. It has, however, recently been done. If helium is cooled below the λ -point (2.172K, the transition to the superfluid state) interesting turbulence effects occur due to the tangling of vortex tubes and its convection properties change significantly [1].

2.2 The Critical Temperature Difference

It is the temperature difference between the two plates that determines whether convection will take place or not. The crucial parameter in Rayleigh-Bénard convection is the Rayleigh number which was derived in 1926 by Lord Rayleigh. Let us consider a sphere of fluid which is ΔT kelvin warmer than its surroundings. This sphere will probably be less dense than its surroundings and so an Archimedian force will tend to push it upwards. This force will be [4]

$$F_A \sim g\alpha\rho_0 r^3 \Delta T ,$$

where α is the volumetric coefficient of thermal expansion, g is the gravitational field strength ρ_0 is the constant density of the surrounding fluid and r is the radius of the sphere. The viscous force resisting the motion is given by Stoke's law:

$$F_S \sim 6\pi r v \eta$$

where v is the sphere's velocity. If the two forces are equal the time it will take the sphere to travel a distance h is

$$t = \frac{h}{v} \sim \frac{6\pi h \eta}{g\alpha\rho_0 \Delta T r^2}.$$

Motion is sustained if the thermal time scale is larger than this. The $1/r^2$ relationship suggests that a larger sphere would convect more easily and so would a warmer one. If we make it as large as possible, i.e. $\sim h$, and make ΔT the temperature difference between the two plates, it follows that the stability limit is given by:

$$A < \frac{\alpha g h^3 \Delta T}{\nu D_T} = R \quad (1)$$

where A is constant [4]. The right hand side is what Lord Rayleigh took as his Rayleigh number, R . The inequality implies that there is a minimum Rayleigh number for which convection can occur. This Rayleigh number is called the absolute critical Rayleigh number or R_{crit} . This is a universal value for all fluids and is equal to 1707.76 [1]. I use the word absolute because it is only exact if the plates and fluid extend horizontally to infinity. The Rayleigh number is proportional to the cube of the height of the convection chamber. It follows therefore that the critical temperature difference, ΔT_{crit} , between the plates for the initiation of convection is proportional to $1/h^3$. The expansion coefficient, the kinematic viscosity, and the thermal diffusivity are all functions of temperature. In all calculations we have to take these quantities as being constant throughout the chamber otherwise they become too complicated. The assumption that only the density is allowed to vary with temperature is called the Oberbeck-Boussinesq approximation. The fluid in our experiment was water. The coldest temperature that the water is ever likely to be at is room temperature, which is normally close to 20°C. The highest temperature liable to be applied to the top plate is about 50°C. Table 2 displays some important data between these two temperatures.

TABLE 2 – SOME IMPORTANT PROPERTIES OF WATER [6, 7].

$T / ^\circ\text{C}$	$\alpha / 10^{-4} \text{K}^{-1}$	$\nu / 10^{-3} \text{Nms}^{-2}$	ρ / kgm^{-3}	$C_P / \text{Jkg}^{-1}\text{K}^{-1}$	$k / \text{Wm}^{-2}\text{K}^{-1}$
20	2.1	1.00	1002	4207	0.604
25	3.0	0.84	1003	4206	0.610
30	3.4	0.78	1004	4204	0.618
35	3.4	0.71	1006	4201	0.626
40	3.8	0.65	1007	4196	0.632
50	4.3	0.54	1011	4191	0.643

The density, the specific heat capacity and the thermal conductivity do not change significantly over the temperature range, and so neither does the thermal diffusivity. The viscosity does however vary significantly and the expansion coefficient more than doubles over the range. We have to assume though that at any one time these properties are the same throughout the fluid and correspond to the average temperature. This normally means that the relationship between R and ΔT is not as linear as we would like it to be.

The only changeable parameter in the Rayleigh number equation is the height. For experimental purposes it is important that we chose a sensible height. Some values of critical temperature difference are displayed in table 3 for different fluid heights. For the case of water at ΔT_{crit} has been given for several chamber heights taking the 35°C values from table 2. Clearly if the height is too small ΔT_{crit} becomes ridiculously large. If $h = 1\text{mm}$ ΔT_{crit} is still too large; we would like to raise ΔT up to 20 times the critical value or more. If $h = 100\text{mm}$ ΔT_{crit} is rather too small to measure reliably. If $h = 10\text{mm}$ ΔT is not too small but it is difficult to get good shadowgraphic images. The range of acceptable chamber heights is therefore rather small, and we have to know it accurately.

TABLE 3 – CRITICAL TEMPERATURE DIFFERENCES [1, 4, 5]

FLUID	h / mm	$\Delta T_{crit} / ^\circ\text{C}$
Air	10	17
Liquid helium (2.3K, SVP)	0.7	0.0095
Carbon Dioxide (300K, 40bar)	0.5	1.23
Silicone oil	10	2.2
Water (20°C)	100	1.2×10^{-4}
	10	0.12
	3.2	3.8
	1	120
	0.1	120000

The height of our chamber was 3.2mm. This measurement was carried out by B. Hof with a travelling microscope. The error on this measurement should be of the order of 1 micron. Table 4 shows how we should relate the Rayleigh number to the temperature difference, which we can measure.

TABLE 4 - ΔT TO RAYLEIGH NUMBER CONVERSION

DT / °C	Average T / °C	R
3.8 (ΔT_{crit})	20.75	1707
10	5	6800
20	30	16500
30	35	31300

Another definition of the Prandtl number is the ratio of the vertical thermal diffusion time upon the viscous entrainment time of the fluid. The characteristic vertical thermal diffusion time for a chamber of height h is [3]:

$$\tau = \frac{h^2}{D_T} .$$

For our chamber, this characteristic time is just over a minute. In other experiments this characteristic time might be much longer and one might have to wait for at least this time for an expected pattern to appear having altered ΔT . If the Prandtl number is small, it will take a relatively long time ($> \tau$) for the fluid's velocity field to adjust to its equilibrium state once the temperature field within the fluid has reached its equilibrium state. It may take a long time for convection to cease when ΔT is dropped below its critical value. In addition to that, the value of ΔT_{crit} is also only correct for situations when ΔT is increased from below ΔT_{crit} . When ΔT is being decreased the critical temperature is often lower, and thus we have a hysteresis effect. To be sure of terminating convection one may have to decrease ΔT to well below ΔT_{crit} and then wait for a while.

2.3 The Oberbeck-Boussinesq equations

The motion of the convecting fluid is governed by three continuity equations, known as the Oberbeck-Boussinesq equations, and the rigid-rigid boundary conditions. Let us first consider the mass continuity equation:

$$\frac{\partial \rho}{\partial t} + \nabla \cdot (\rho \mathbf{v}) = 0 .$$

The Oberbeck-Boussinesq tells us that the first term is zero. If the temperature remains constant the density cannot change with time. If we assume that the fluid is incompressible, which is normally reasonable when talking about a gas as density gradients are never very large, then $\nabla \rho$ is 0. This leads to the first Oberbeck-Boussinesq equation, which is,

$$\nabla \cdot \mathbf{v} = 0 .$$

The second equation comes from the heat diffusion equation, which is,

$$\frac{\partial T}{\partial t} + \mathbf{v} \cdot \nabla T = D_T \nabla^2 T .$$

We can rewrite this equation in terms of the perturbation of the temperature, θ , from what T would be if there were only conduction taking place and no convection (see figure 1). That equation is, after appropriate rescaling,

$$\frac{\partial \theta}{\partial t} + \mathbf{v} \cdot \nabla \theta = R \mathbf{v} \cdot \mathbf{k} + \nabla^2 \theta . \quad (2)$$

This is the second Oberbeck-Boussinesq equation.

The final equation comes from the Navier-Stokes equation,

$$\rho \left(\frac{\partial \mathbf{v}}{\partial t} + (\mathbf{v} \cdot \nabla) \mathbf{v} \right) = \rho \mathbf{g} - \nabla P + \eta \nabla^2 \mathbf{v}$$

where P is the pressure. If we do the same thing for the pressure that we did for the temperature and define Π as the pressure perturbation from the conducting state we can obtain the third equation [1]:

$$\frac{1}{Pr} \left(\frac{\partial \mathbf{v}}{\partial t} + (\mathbf{v} \cdot \nabla) \mathbf{v} \right) = \theta \mathbf{k} - \nabla \Pi + \nabla^2 \mathbf{v} \quad (3).$$

In the case of the infinitely extending horizontal parallel plates the boundary conditions are as follows. At the plates' surfaces:

$$v_z = \frac{\partial v_z}{\partial z} = \theta = \Pi = 0.$$

v_z has to equal zero next to the plates because no fluid can move through them. These boundary conditions are known as the rigid-rigid boundary conditions. The patterns observed are the solutions to the equations according to the boundary conditions. In the conducting regime the v 's Π 's and θ 's are equal to 0 everywhere and the solution is trivial. For stable or time-independent convective flows the second order terms, $(\mathbf{v} \cdot \nabla) \theta$ from equation 2 and $(\mathbf{v} \cdot \nabla) \mathbf{v}$ from equation 3, are small compared to the linear terms and are thus neglected in calculations. In that instance it can be seen from equation 3 that fluid acceleration is proportional to Pr . As the second order terms become larger for higher Rayleigh numbers the time-dependent flow becomes more important.

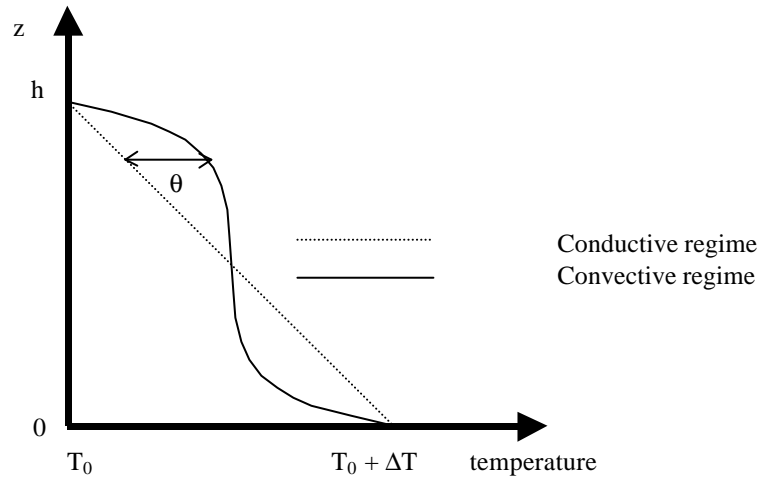


Figure 1. Temperature profile between plates (averaged over the width) in conductive and convective regimes [1].

2.3 The Bifurcation at the onset of convection

The transition between conduction and convection is phase transition and we can apply the Landau approach to it. Velocity is taken as the order parameter. Let us invent a pseudo-potential, ϕ :

$$\phi = \phi_0 + a_1 v + \frac{a_2}{2} v^2 + \frac{a_3}{3} v^3 + \frac{a_4}{4} v^4 + \dots$$

where the a -values are constants and ϕ_0 is the potential at the onset of convection, [4]. The Boussinesq-Oberbeck approximation tells us that up-going fluid has the same properties as down-

going fluid and so $\phi(v) = \phi(-v)$. This implies that all of the odd-numbered a values are 0. When close to equilibrium each term in the potential becomes successively smaller and so let us only consider the v^2 and v^4 terms. Stable equilibrium states occur when $d\phi/dv$ is 0 and the second derivative is positive. We therefore have the equation

$$\begin{aligned}\frac{d\phi}{dv} &= a_2 v + a_4 v^3 = 0 \\ v &= 0 \quad \text{or} \\ v^2 &= -\frac{a_2}{a_4}\end{aligned}$$

As we tend to the threshold the $v^2 \gg v^4$. Both of these terms must tend to 0 however and so it follows that a_2 might be proportional to $R - R_{\text{crit}}$. It is in fact

$$a_2 = \frac{R_{\text{crit}} - R}{R_{\text{crit}}}.$$

Figure 2 shows schematically how the potential varies with v for $R - R_{\text{crit}} > 0$ and for $R - R_{\text{crit}} < 0$. The minimum in the red curve represents the stable conduction state, with v equal to 0. The minima in the green curve represent two possible convection states.

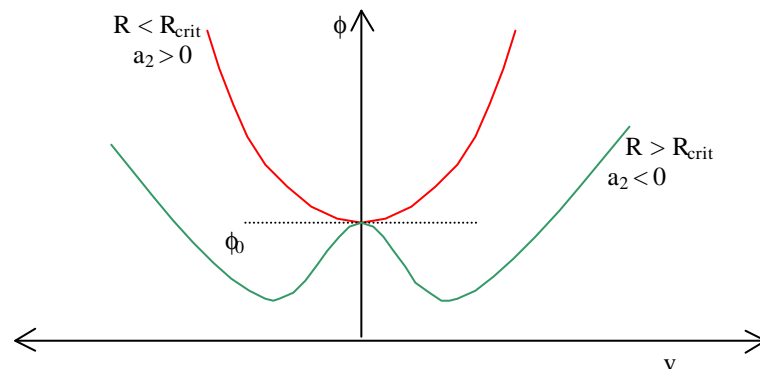


Figure 2 The pseudo-potential with order parameter v .

If we were to plot R against v we have a normal bifurcation, see figure 4. Bifurcation means that there are two possible states that the fluid can move into with equal probability. This normally corresponds overall to two convection patterns that the same in every respect except the motion is reversed. It is called a normal bifurcation because the gradient is infinite at the transition.

We can gain a physical understanding of this bifurcation principle if we reconsider the rising warm sphere of fluid within cooler surroundings. In figure 4 there is a sphere of warm fluid meeting a sphere of cooler fluid. It doesn't know which way it should move in order to pass it.

In any real, one possibility is always more likely than the other due to asymmetry in the apparatus. Alternatively one particular state could be forced manually. One method is to produce a horizontal temperature gradient by gently heating one section of the sidewall [4].

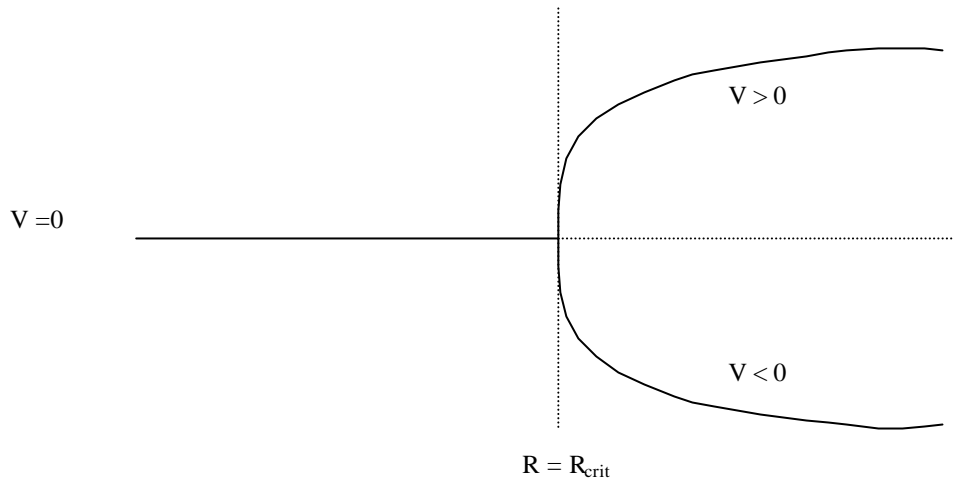


Figure 3. The velocity at any particular point undergoes a normal bifurcation at $R = R_{crit}$.

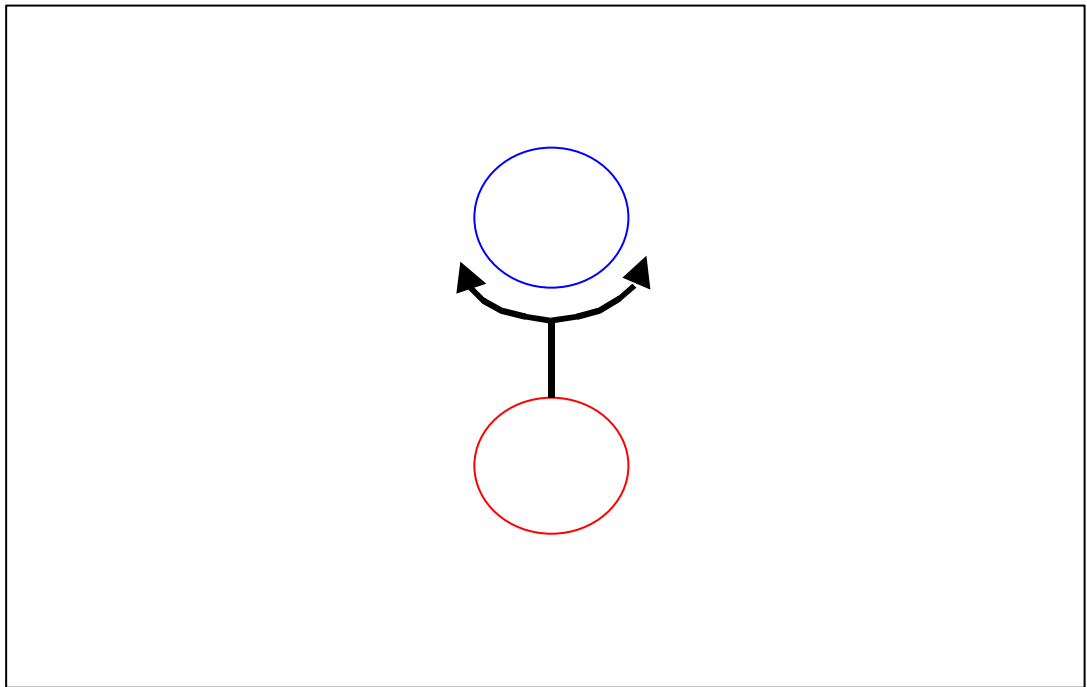


Figure 4. At the onset of convection, the rising sphere of warm fluid (red) meets a falling cooler sphere, and doesn't know which way to move.

If we can measure the velocity field in a fluid we should be able to detect a sudden change at the onset of convection. This is a possible method of measuring R_{crit} . However the velocity field inside a convecting fluid may or may not be measurable. In the case of liquid helium it is very difficult to measure [1]. A more easily measured quantity is the Nusselt number and is defined by the equation:

$$N = \frac{\Phi_V + \Phi_D}{\Phi_D}$$

where Φ_D is the heat flux due to conduction and Φ_V is the heat flux due to convection. When $R < R_{crit}$, $N = 1$. When $R = R_{crit}$, the gradient changes from 0 to infinity. For $R > R_{crit}$ Φ_V is non-zero and

$N > 1$. For higher values of R , N is proportional to the square root of $R - R_{crit}$. If we can measure heat fluxes through the chamber we can deduce R_{crit} .

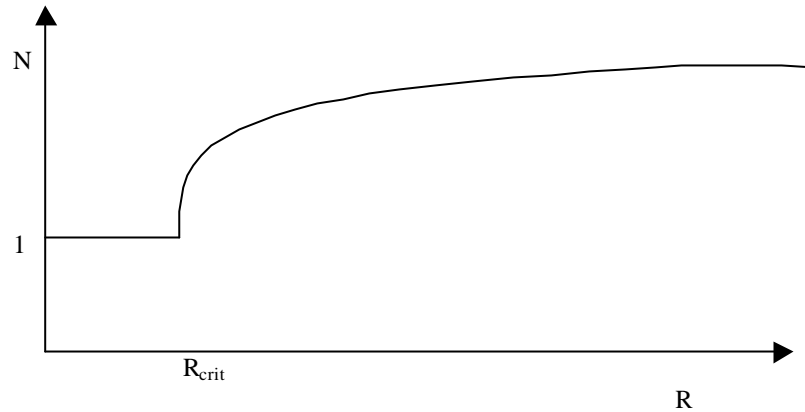


Figure 5. The Nusselt Number suddenly increases from 1 at the onset of convection.

2.3 Straight Roll Convection

The simplest type of time-independent convection solution is the straight roll pattern. The type of motion in question is shown in figure 6. For this type of motion we can define a dimensionless wave number [2],

$$k = \frac{2\pi h}{\lambda}$$

where λ is twice the width of the roll. If the Rayleigh number is just above the threshold a roll pattern is formed with a wave number of 3.117 [1]. This is known as the critical wave number and it corresponds to a roll which is just slightly wider than it is high, by a factor 1.008. Harmonic modes of shorter wavelength may form but they tend to disappear quickly and couple back to the fundamental mode [3]. The graph in figure 7 shows the dividing line, called the marginal stability curve, between the conducting and the convecting zones. If we were to take a line perpendicular to the roll the temperature distribution along this line, averaged over the height d , is approximately sinusoidal [3]. This is known as the mid-height temperature distribution. The equivalent distribution for v_z is also sinusoidal. In 1977, Normand et al. showed, that the distribution is, provided R is not too large,

$$v_z = \frac{D_T}{h} k^2 \sqrt{\frac{2(R - R_{crit})}{B}} \cos\left(\frac{2\pi x}{\lambda}\right)$$

where B is a polynomial function of the Prandtl number and x represents the position along the roll's diameter. Notice that the wavelength is proportional to h . v_z is therefore proportional to h . If $Pr \gg 1$, and for water it is, $B \approx 2031$. Our convection chamber was 3.2mm in height 12.8mm in diameter. Water at 36°C has a thermal diffusivity of $1.51 \times 10^{-7} \text{ m}^2/\text{s}$, [9]. The velocity amplitude at $10R_{crit}$ for water in our chamber is $\sim 0.46 \mu\text{m/s}$, so in our experiment the convective motion is not very quick. By contrast in the outer layers of the Sun convection can reach speeds of over 100 m/s, for the plasma is accelerated over huge distances.

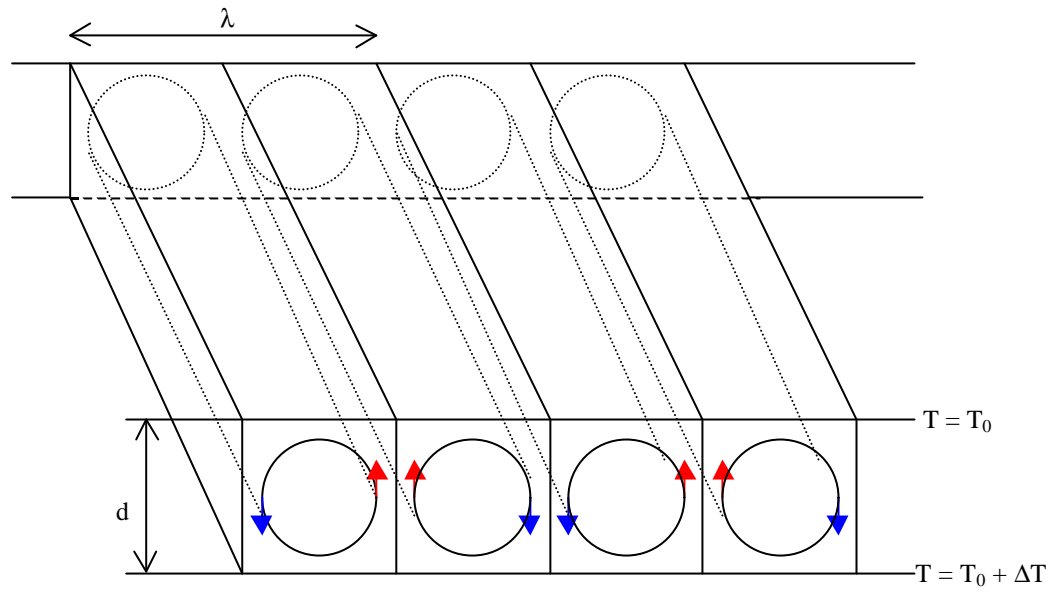


Figure 6. Straight roll convective motion.
The red arrows indicate rising warm fluid and the blue arrows indicate falling cooler fluid.

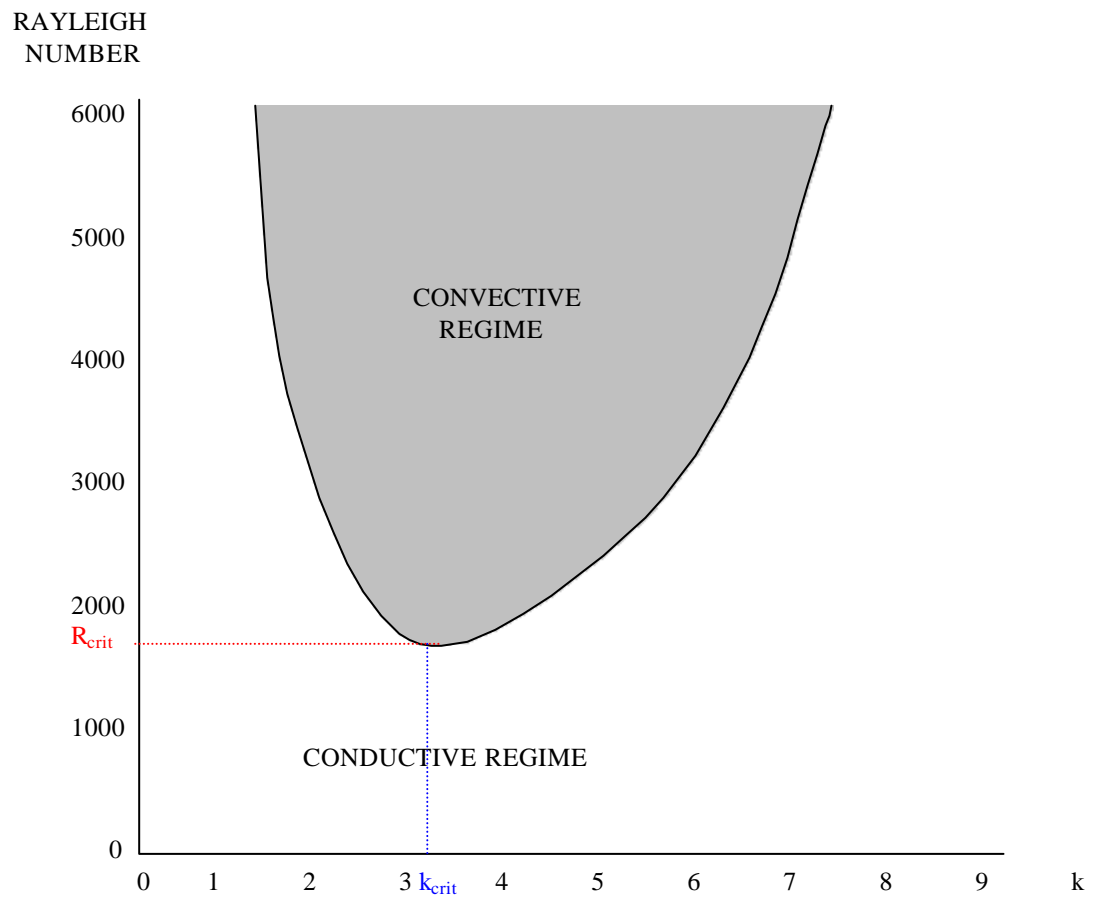


Figure 7. The marginal stability curve, dividing the two main regimes.

2.6 The Effects of the Sidewalls

The graph in figure 7 and the values for R_{crit} and k_{crit} are only correct for an infinitely extending horizontal convecting chamber. For Rayleigh numbers higher than R_{crit} a range of wave numbers are possible. At the onset of convection the rolls settle into one pattern of constant wavelength. None the less, if reasonably close to the threshold, the pattern of wavenumber k_{crit} is the most stable pattern and thus the most likely to form. This is not quite true if there are sidewalls. Close to the sidewalls the rolls' amplitudes are damped [4]. Close to R_{crit} the marginal stability curve can be approximated to a parabola and thus Δk is :

$$\sim \sqrt{R - R_{crit}}.$$

It follows that there should be a corresponding modulation length which is proportional to $1 / \Delta k$. It turns out that if the vertical velocity amplitude is zero at the sidewalls this length is equal to [4]

$$\frac{0.385h}{\sqrt{R - R_{crit}}}$$

Close to the convection onset this distance can be quite large in a tall container. At $R = 2000$ ($1.17R_{crit}$) in our chamber, for example, this is 0.07mm. The diameter of our convection chamber is 12.8mm, and so this effect is negligible in our instance. At higher Rayleigh numbers the modulation length shortens and becomes even less important.

For a cylindrical chamber of aspect ratio greater than 10 it is reasonable to consider the diameter as infinite [8]. Our convection chamber had an aspect ratio of 2.0. The result of this that drag forces due to the sidewalls are significant and thus R_{crit} is little higher, this is a result of what is called dynamic sidewall forcing [9]. New boundary conditions are introduced, at the sides of the chamber

$$v_r = \frac{dv_r}{dr} = \theta = \Pi = 0.$$

where v_r is the radial velocity outwards from the centre.

The critical Rayleigh number is plotted against the aspect ratio in figure 8. This curve is in fact built up from a set of curves which each correspond to a stable convection pattern type [10]. The two most important have been ones marked out in solid lines where they form part of the ' R_{crit} vs. Aspect ratio distribution' and with dotted lines where they are above the main curve. The green curve corresponds to an axisymmetric mode. The blue curve correspond to an asymmetric mode [10]. There are at least two other curves, which also correspond to asymmetric modes, which just graze the surface of the main distribution at one or two places within the range shown. They have not been drawn for there is little to be gained in doing so. The 'chinks' in the main curve are where it is relatively difficult to 'fit in' any particular pattern remembering that a roll's diameter is approximately equal to its height. It should be noted that only for aspect ratios < 1 is the critical Rayleigh number very much higher than the absolute value.

Our chamber has an aspect ratio of 2 and links up with curve one. This suggests that an asymmetric mode forms at the onset of convection, most probably a straight roll pattern. We can deduce that the critical Rayleigh number in our chamber is ≈ 1860 . This correspond to a critical temperature difference of 4.1°C . As the width of a fundamental roll is just slightly larger than its height (not the case for the harmonic rolls), there is almost enough room for 4 rolls, but not quite. We therefore expect the most stable pattern to be one with three rolls.

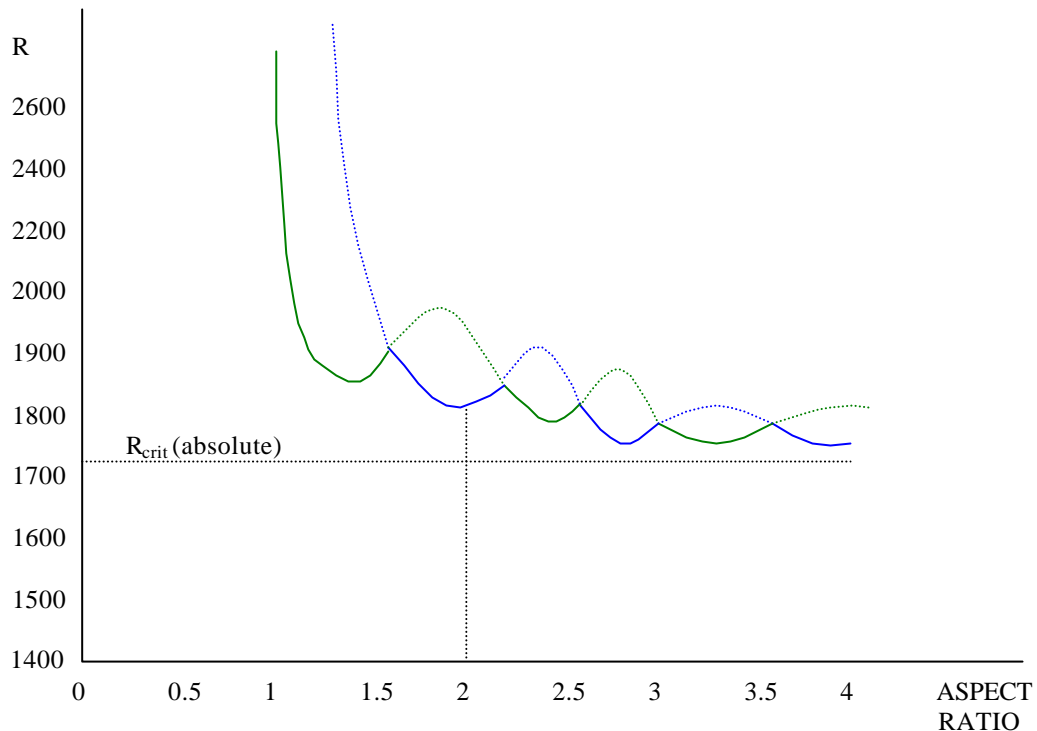


Figure 8. Critical Rayleigh numbers for cylindrical convection chambers with insulating sidewall, [10].

Convection rolls in a cylindrical chamber like to terminate at right angles to the sides. This results in the ends of the rolls being somewhat curved. Figure 9 shows a convection chamber where a three-roll pattern is in operation. The three rolls are divided by dotted lines. The regions of rising hot fluid are shown in red and the falling cooler regions are in blue. No indication of the speed of the fluid's motion is given in the picture, and this is not the kind of image that shadowgraphy produces.

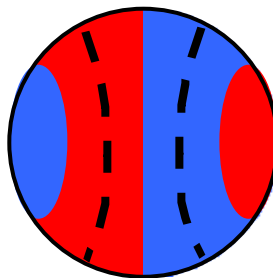


Figure 9. A three-roll pattern in a cylindrical container of small aspect ratio. The dotted lines divide the three rolls. The red areas represent warm fluid rising and the blue areas indicate cool fluid falling.

2.7 Busse Balloons and Time Dependent Flow

The stability of a straight roll pattern is not simply defined by the marginal stability curve. It is defined by the Busse balloon, named after F. H. Busse [11]. Figure 10 shows the Busse balloon for a fluid of Prandtl number in an infinitely extending chamber. The Prandtl number of water is temperature-dependent, but it is reasonable to apply this Busse balloon to water. The dotted line is the marginal stability curve. Stable straight roll patterns can only exist within the area enclosed by the solid lines. The rolls become unstable if we try to move out of the Busse balloon. Changing the wavenumber of a roll pattern is not easy in a chamber of fixed size, though under some circumstances it can be done. As there was almost enough room in our chamber for four rolls. By

manually perturbing the system we might be able to squash the three rolls and make room for a fourth to appear. If we were to move to the left on the diagram to the cross roll line, initially small rolls perpendicular to some of the main rolls will form. Then, perpendicularly to one of the small rolls, another roll will appear. That eventually becomes another long roll. The number of rolls has increased in the process and so has the wavenumber [2]. When moving across the skewed varicose instability the reverse happens. First the pattern becomes distorted, and then some adjacent rolls merge together and the wavenumber decreases [2]. If the skewed varicose is approached very quickly though the pattern could break down into a disordered time-dependent state. If we attempt to cross the knot instability line, spokes start to grow out from the rolls and so a spoked pattern may develop [10]. This can be done by simply boosting the Rayleigh number, but it only works for water if the wavenumber is within a small range. Figure 11 shows the Busse balloon for air, which has a Prandtl number of 0.7. An instability known as the oscillatory instability is marked. On crossing that line waves start to propagate along the rolls and we have time-dependent flow. For water this line does not enter the Busse balloon. Generally speaking, time-dependence sets in when going off the top of the Busse balloon. Fluids of low Prandtl number enter time-dependence at lower Rayleigh numbers than do fluids of high Prandtl number. In the case of liquid metals, time-independent flow can only take place within a narrow range of Rayleigh numbers, due to their exceptionally low Prandtl numbers.

It should be stressed that the Busse balloon is only strictly correct for long straight rolls. In our experiment any convection rolls produced will not be very long and not be very straight. The Busse balloon should therefore not be used a general purpose ‘roadmap’ for producing particular patterns in our instance. It seems reasonable to assume though that time-dependence sets in between $R = 20000$ and $R = 30000$.

2.8 Other Time-independent Patterns

In the previous section I mentioned spoked patterns. In these patterns upward (or downward) flow takes place along spokes that probe outwards from the centre and the reverse motion takes place around the edges of the cell. In our chamber we should be able to produce patterns such as the cross (4 spokes) and the ‘Mercedes sign’ (three spokes).

Another type of stable pattern that might be formed is the concentric ring pattern. If the thermal diffusivity of the sidewalls is equal, or at least nearly equal, to that of the fluid these patterns should never be produced unless the vertical walls are deliberately heated or cooled. That ensures that the fluid either rises or falls at the edges [9]. If the sidewalls are not thermally coupled to the top and bottom plates properly, or if the diffusivity of the sidewalls differs greatly from that of the fluid it is possible to produce concentric ring patterns at least temporarily. For example, suppose ΔT is increased rapidly from below ΔT_{crit} to a value which is several times ΔT_{crit} and the thermal diffusivity of the sidewalls is greater than of the fluid and the contacts are good. The value of θ everywhere on the sidewalls is positive and so upward motion will take place there. Downward motion must take place further in and so at least one convective ring is formed.

In the case of silicone oil, the viscosity varies significantly with temperature. This means that even for a fairly modest ΔT the Rayleigh number is larger nearer the warm plate. As a result it is quite easy to produce hexagonal patterns. Fluid rises in the centres of hexagons and drops down at the sides.

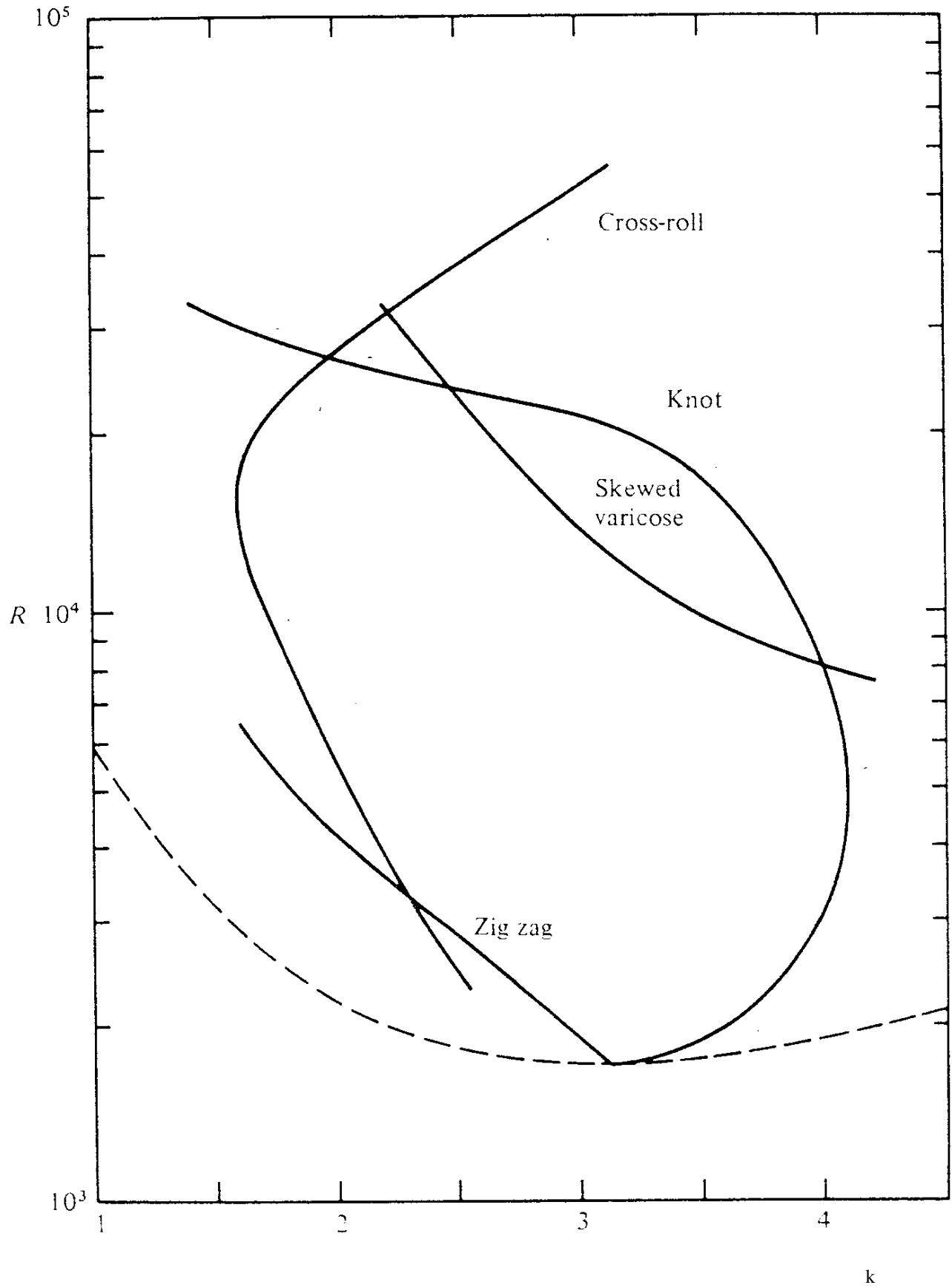


Figure 10. The Busse balloon for a fluid with $Pr = 7$. [11].

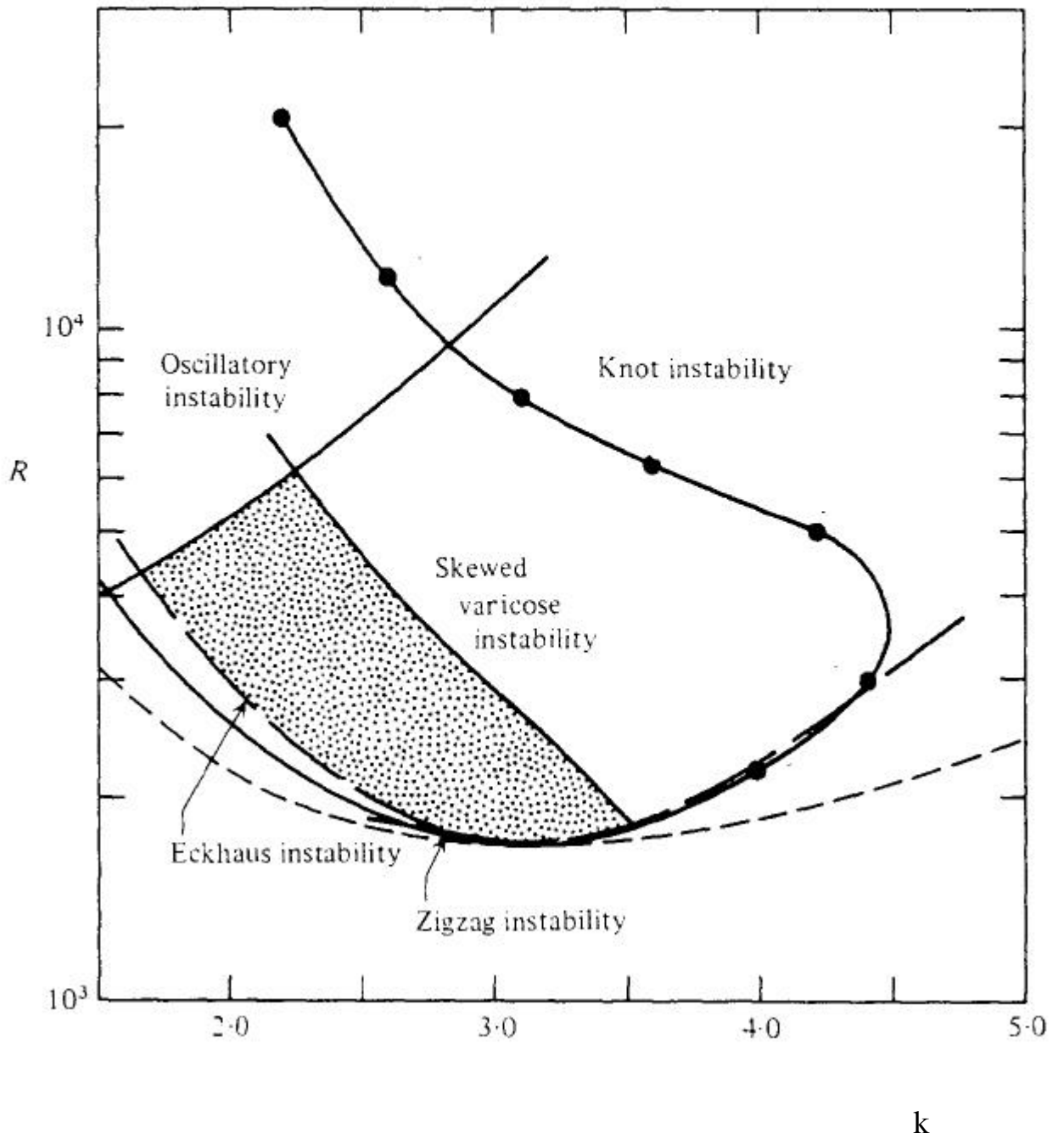


Figure 11. Busse balloon for air. $Pr = 0.7$ [11].
The stable area for straight rolls is shaded.

3. SHADOWGRAPHY

3.1 SHADOWGRAPHY Vs SCHLIEREN

There are two main methods of observing the flow patterns in a convecting fluid, these are the shadowgraph and schlieren techniques. We use shadowgraphy in our experiment, although the choice of technique can often be very difficult; the majority of experiments use the shadowgraph technique. The main advantage of the shadowgraph technique is that the image created differentiates between hot or rising fluid and cold falling fluid, measuring the second differential of the refractive index with respect to a distance, dn^2/dx^2 [2]. The schlieren technique however offers an experimentally much simpler set-up, and in many cases it can produce a more contrasting image, however it only measures the first order differential dn/dx .

The shadowgraph technique is based on the principle that the refractive index of the fluid increases linearly with temperature, at least over small temperature differences. The mid-height horizontal sinusoidal temperature distribution across a roll should thus lead to a corresponding distribution in refractive index. If a beam of parallel light is shone through the convection cell the convection rolls act like converging and diverging lenses, and so cause the light to be deflected. It is then possible to produce an image of the deflected light after it has passed through the cell, on a charge coupled device (or otherwise) with light and dark areas indicating where the fluid is rising or falling.

The application of both these methods is not restricted to convective fluids but has many uses in the study of shock waves and cavitation. In more recent years people have tried to design apparatus that may allow the visualisation of quantised vortex lines in liquid helium to take place, there has been little success so far but is a very interesting area of research.

3.2 THE TWO-LENS SYSTEM

In the past the majority of investigations into Rayleigh-Bénard convection utilising the shadowgraph technique, have used a basic two-lens set-up. Indeed the apparatus we inherited was the two-lens system first described by Croquette, and taken from [12], see figure 12 below.

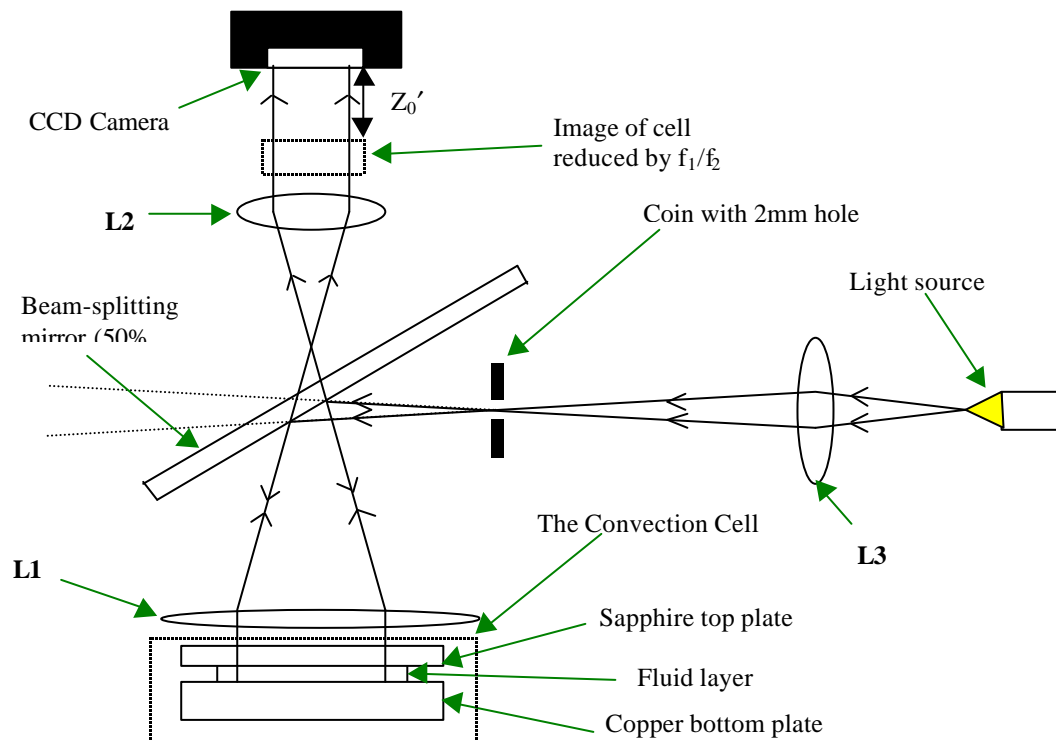


Figure 12. The original 'two' lens Croquette system.

The lower of the two conducting plates was made 8mm thick copper with a reflective coating of nickel-chromium alloy, the top plate was a 3mm thick window of sapphire, which was in contact with the fluid layer, thus keeping the upper boundary at a constant temperature. The reasons for using sapphire, are its transparency and its high thermal conductivity. We would ideally like to have perfectly conducting top and bottom plates, so that the fluid layer is in perfect thermal contact with the confining plates, and their immediate surroundings. The purpose of L3 and the pierced coin was to synthesise a point source. If too much extraneous light enters the system then the images obtained could have a significant reduction in contrast. To reduce the amount of light leaking into the apparatus we covered the vertical optical stand with a red cardboard light shield; it was noticeable to the eye that this improved the overall contrast of the image.

In this system the lenses produce an image of the cell between L2 and the camera. The distance from this image to the camera face is denoted by Z_0' . It is over this distance that the shadowgraphy takes place. If there were no lenses at all in the set-up, this distance would just be physical gap between the convective fluid layer and the CCD camera screen; this distance is called Z_0 . The two are linked by the magnification effect the lenses have on the cell image thus [2]:

$$Z_0 = \left(\frac{f_1}{f_2} \right)^2 Z_0'$$

where f_x indicates the focal length of lens x . Now the distance over which the shadowgraphy can take place has been drastically reduced by the introduction of lenses L1 and L2. The action of these two lenses is to reduce the size of the image, and to heighten the overall contrast of the image, the extent to which this happens is dependent on the ratio f_1 / f_2 . This puts forward a hard choice for the experimentalist, on one hand an increase in contrast may contribute significantly to the ability of the system to visualise patterns. But on the other a tiny image with excellent contrast will help nobody. So a balance is found and we are made acutely aware of the reduction this causes to the overall system resolution.

The problem of such a trade-off was accepted as part of the method necessary for imaging convective flows. Many experimentalists positioned the optics of their experiment so that the light emerging from the eyepiece lens L2, was slightly diverging to the extent that when it reached the camera it would entirely fill the entrance window. This is a practical way of preventing the reduction of the image to an impractical size. However it does have its disadvantages, when parallel light is transmitted from the eyepiece, the camera may be placed at any distance from the new image of the cell, this means that it is possible to vary Z_0' (and hence Z_0) without altering the image size. To understand why this is useful, it is necessary to think of the convective cell as a line of alternately converging and diverging lenses, see figure 13 [5]. This view implies that the cell would have an overall focal length F , this being the distance from the cell at which the light is concentrated into a single line for each bright region, and the reverse for the dark regions.

Therefore as we see from figure 13, placing the camera at a distance from the image of the cell, which is less than F , we would see bright, blurred lines in the image. If we moved the camera so that it was placed a distance F from the image of the cell, we achieve the maximum possible contrast for the system. Placing the camera further from the cell image than F will result in a sharply contrasting image, with double lines where there had previously only been single. So the ability to move the camera, without altering the image size, but changing the contrast is known as the optical lever effect. There is an optical lever effect only as long as the distance F is not exceeded.

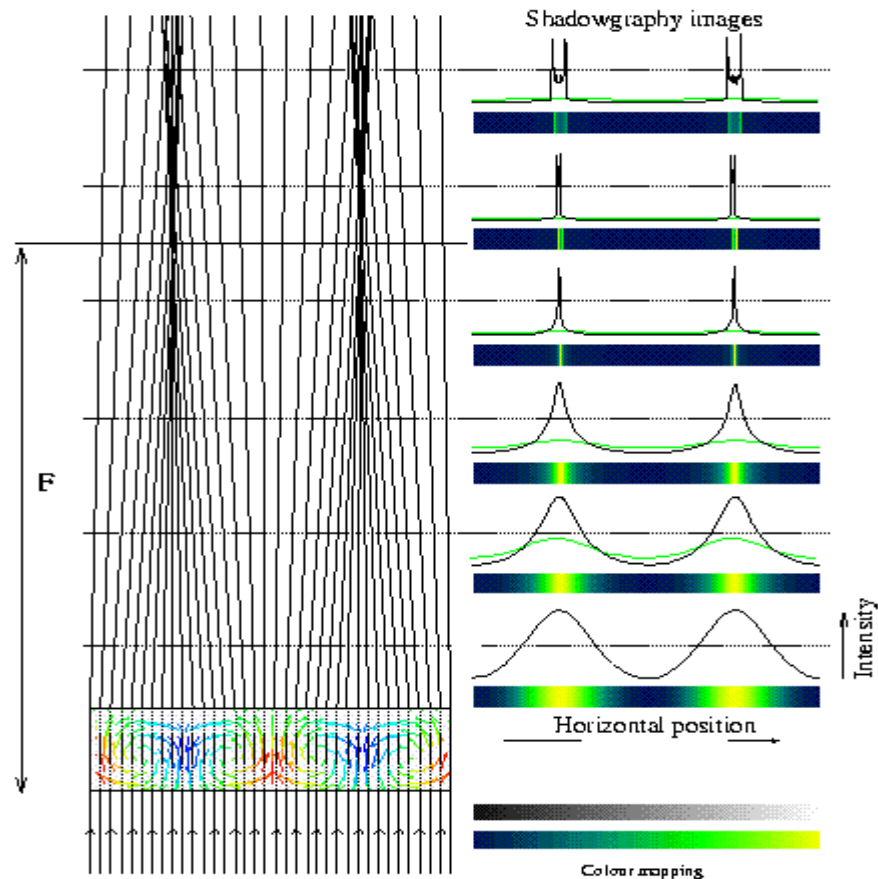


Figure 13. The convective cell has an overall focal length or focalisation distance F [5].

3.3 THE FOUR-LENS SYSTEM

A system that would seem to solve this problem has been described by Croquette [2]. In this system he utilises two extra lenses in the main optical path between the old lenses and the CCD camera. These would allow the image of the cell to be resized to any value, dependent upon the focal lengths of the lenses chosen, and hence enlarged to fully fill a detector. The action of the new lenses is solely upon the image size and no reduction in contrast is expected from the two-lens case. We aim to assemble this system and compare the images taken with the old two-lens set-up with those taken by this new assembly. If the four-lens system can increase the image size with no deterioration in contrast compared to the two-lens system, there are plans to employ the new system in the next generation of cryostat in the low temperature convection group.

The apparatus that we used was a collection of several parts designed by MSc and PhD students from previous years. In this way we have inherited a well modified and working apparatus. The most recent of these modifications were carried out by Bjorn Hof as an MSc project. He investigated the effects of a tilted or angled convection cell on the pattern formed [12], and the stability of patterns in a small aspect ratio cell [12,13], using the two-lens Croquette system previously described.

Consulting the notes we had for the construction of the four-lens Croquette [2] system, it was evident that the majority of the apparatus was already in place and that only minor physical modifications were required. It was possible to utilise the upright section of the apparatus to house the extra two lenses, and our initial worries over the available space were allayed by careful lens choice as will be shown later. However in order to mount the lenses on the upright bars two new clamps had to be fabricated. We were able to re-use the design of an existing part of the apparatus with only minor alterations, removing the need to design any new parts and allowing the technicians to make the parts immediately.

Both the lenses were to be held within the usual optic mounts, however the screw threading on the available mounts were wrong, as well as the overall mount being too long. Again the technicians proved to be our solution, re-threading the foreshortened mount to suit our needs exactly. Figure 14 shows the set-up of our new system in terms of the focal lengths of the lenses involved. The system produces an image of the cell between the lenses L2 and L3. Lens L3 effectively views this image of the cell (Z_i) from a distance Z_0' away, the combination of lenses L3 and L4 then simply expands out the image of the fluid cell. The optical alignment is such that a parallel light beam is emitted from L4, so that the optical lever effect may be used.

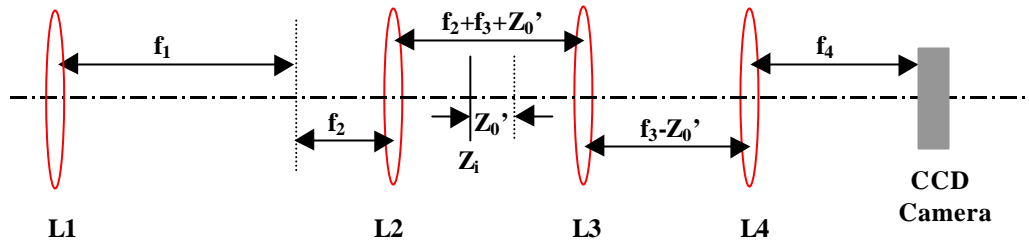


Figure 14. The four-lens system layout, in terms of lens focal lengths.

When the two lenses L3 and L4 resize the image, it can be expanded to any size, optimally we would like to make it as big as possible on the CCD camera. The size of the image on the detector is equal to the diameter of the cell multiplied by the factor F :

$$F = \left(\frac{f_4}{f_3} \frac{f_2}{f_1} \right)$$

This is a highly useful result, allowing anyone to resize their cell images without resorting to the divergent beam approach, and thus allowing them to make use of the optical lever effect. In order for us to make full use of the camera we required the image to be as large on the CCD as possible.

With the exception of refilling the fluid cell and cleaning the components to ensure that no contaminants were getting into the system, convection cell as a whole was unaltered from that used in previous work. The Sapphire plate that we have as the upper boundary of the fluid layer is a component that must be correctly installed; it is vital that the top of the plate remains in good thermal contact with the cooling water, and the bottom plate with the heater mat and the lower fluid boundary. Failure in this regard would cause the differential thermocouple, which is thermally anchored to both plates to give an incorrect value for the temperature difference across the fluid layer. We controlled the temperature difference across the fluid layer by means of a water pump and a power supply. The water pump we used had a heater built-in so we could alter the temperature of the water used to cool the upper boundary plate and the top of the liquid layer. Increasing of the Rayleigh number was done by manipulation of the power fed to the heater mat, however due to the time it took for an increase in mat power to reach all the cell it was necessary to wait after any power change to gauge its effect. This was no problem when making large changes, but when trying to stabilise a pattern at a given temperature difference, it was a severe handicap. Figure 15 shows the convection cell we used, indicating the main components.

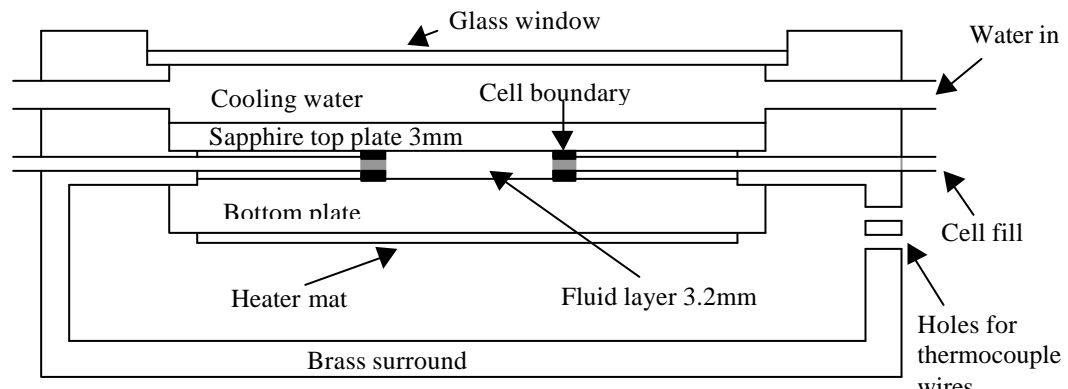


Figure 15. Diagram of the convection cell.

3.4 LENS SELECTION

We chose our lenses L1 and L2 from those available to us (being the more expensive to buy), and decided what values of L3 and L4 were required to maximise the image size with respect to the CCD size. In the end we had to order a new lens so that we could make the image large enough, we ordered a lens with a focal length of 30mm but with a diameter of only 25mm. This allowed us to create large cell images on the CCD screen, although the bowing of the front face of the lens will introduce more spherical aberrations into the experiment. The final lens selection is shown below:

TABLE 5. DATA FOR THE FOUR MAIN LENSES IN OUR SYSTEM.

Lens Number	1	2	3	4
Focal Length (mm)	500	30	30	75
Diameter (mm)	102 (4")	12.5	25	25

After selecting the components we calculated the positions that each element of the system would need to be in for optimal imagery, these are shown in figure 14. We positioned the new components in the system, and tried to align the optics with the conventional car bulb (55 watt) light source. However it proved very difficult in all conditions but a total blackout to actually see the image that was transmitted to the camera, with the bulb having such a diffuse and poorly defined beam. We used a Helium-Neon laser to help us align our optics correctly, it having a small and well-defined beam. This proved to be very successful, enabling us to identify and eliminate some spurious reflections from the metal apparatus as well. We found it considerably more difficult to align the four-lens system than the two-lens one, particularly aligning L3. Figure 16 shows images from both the four and the two-lens case, and in both it is possible to see the worst of our spurious reflections, in the bottom right of the right hand image, and the top middle of the left hand image. It is also possible to get a feel for the scale of image expansion that is afforded by the new optical system.

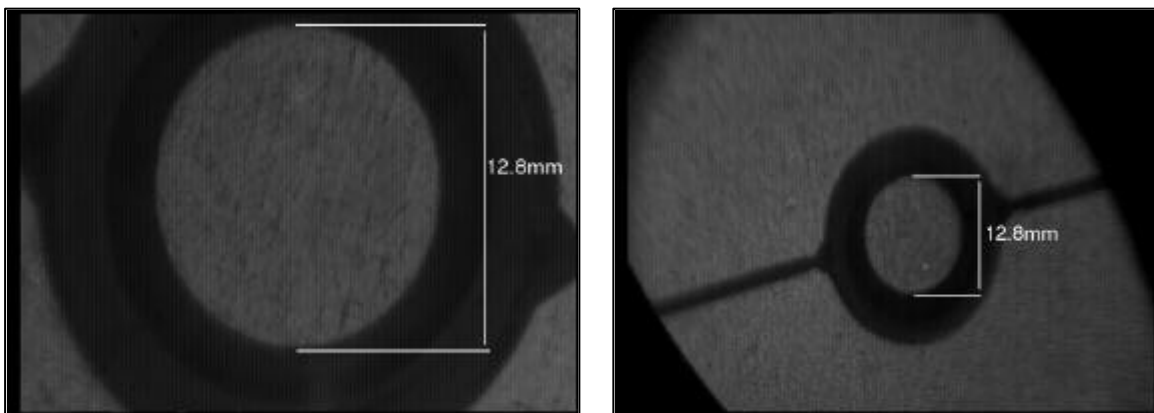


Figure 16. Images of the non-convecting fluid cell, showing the main unwanted reflection.

Another problem we encountered was that the convection cell required very careful filling. The cell was simply filled with purified water, but to avoid the problem of bubbles forming inside the cell the majority of the air was removed from the water prior to the cell fill. This was done with a rotary vacuum pump. When the air had been removed the water was put into a syringe and this was attached to one side of the cell fill line. The other side was pumped on with the rotary pump to create a small pressure imbalance. We used this imbalance to draw the water through the cell and thus reduce the size and number of bubbles formed whilst filling. It was practically impossible to remove the smallest of the bubbles, but these would dissolve back into the water over time; we could then begin to take clear pictures.

4. EXPERIMENTATION

4.1 PREVIOUS EXPERIMENTS

Previous investigations into convective patterns with this convective cell [12,13], have produced excellent images of the many varied types of convective pattern that have been found. The patterns have been found to be stable in a range of Rayleigh numbers, from 3500 right up until the onset of time dependent instability at a Rayleigh number of around 20,000. Figure 17 shows the regions of stability, and the way in which patterns could be formed for the most common patterns described in [12,13].

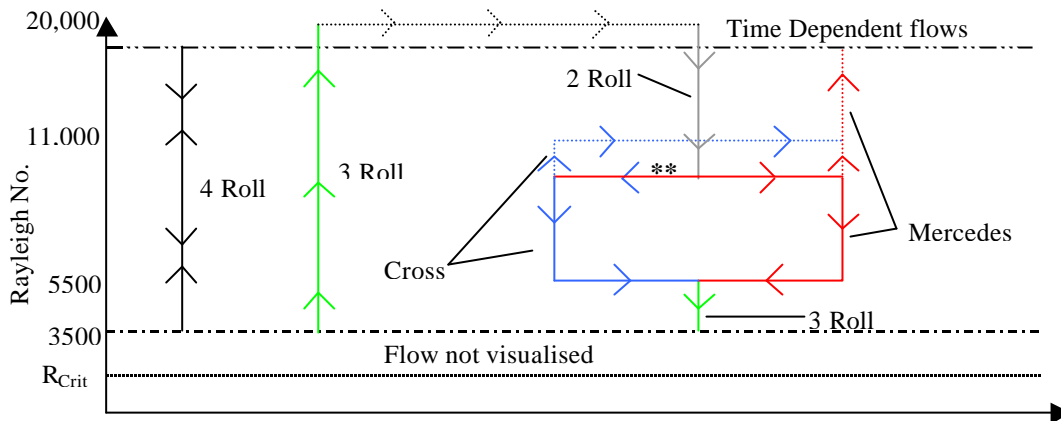


Figure 17. Stability regimes and evolution of the basic patterns found by Bjorn Hof [12,13].

The patterns shown in figure 17 are all stable for any given length of time, other patterns were discovered but were found to be unstable over long time periods. In figure 17, the arrows represent the direction of change in the Rayleigh number, so to create the Mercedes pattern, it is required to reduce the Rayleigh number from time dependence to approximately 11,000 where the bifurcation to the new flow pattern takes place. Below the value of R_{crit} no convection takes place, and between R_{crit} and $R = 3,500$ convection should be taking place, but it is not visualised. The dotted paths represent the hysteresis effect in the bifurcations, often some flow states are stable at a higher Rayleigh than that at which they are formed, a prime example of this is the Mercedes pattern, which is formed from the two-roll pattern at $R = 11,000$ but then remains stable until time dependence sets in at $R = 20,000$. The path to the cross pattern is marked ** because this is not the normal end product of the bifurcation at $R = 11,000$, but can be achieved by boosting the heater power by 1 watt at the point of bifurcation.

4.2 EXPERIMENTATION WITH THE FOUR-LENS SYSTEM

Our next aim was to try and reproduce some of the patterns that had been observed by Hof [12], and Hof et al [13], with our working four-lens optical system. The initial set-up with the four-lens system allowed us to image the convective flows, and so we attempted to follow the steps given in [12, 13], for the creation of the basic flow states. Some of the basic flow states that we found are shown in figure 18; the spurious white reflection is also visible in the first of the three images. When we first increased the Rayleigh number to visualise the flow, we saw a three-roll pattern, confirming our expectations in this regard.

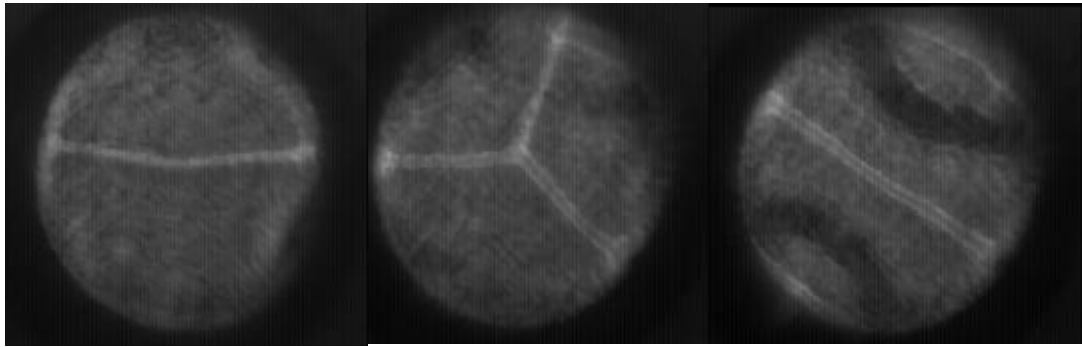


Figure 18. Two roll, Mercedes and Four roll pattern images taken with the four-lens system.

However when we attempted to reproduce some of the flow patterns that had more complicated histories, we were unable to create the flow in its steady state. The starting point for these patterns was the concentric ring pattern, in our cell we only expected to see one or two rings when the pattern was formed. To create this pattern we rapidly changed the Rayleigh number in a discontinuous jump, from below the critical value to around $7R_{\text{crit}}$. If we continue to increase the Rayleigh number as quickly as possible, we should then create one of the two previously seen spoked patterns. We managed to create the ring pattern, with both a white spot and a black spot at the centre, however on further increasing the Rayleigh number we never managed to create any spoked patterns. With further investigation into the experimental method of previous works we discovered that, often even if the parameters are correct the fluid layer may not start to convect in a particular flow state unless the previous state has been disrupted, allowing the new one to form. We found that the best way to disrupt the fluid layer was to squeeze the water fill line that was attached to the fluid cell, thus injecting water across the layer and destroying any current flow state. New flow patterns could then easily form from the remnants of the old flow state.

Now we were able to reproduce all but the extremely difficult patterns from previous experiments. Images of these flow states, the two, three and four-roll as well as the Mercedes pattern taken with the four-lens system are shown in figure 19.

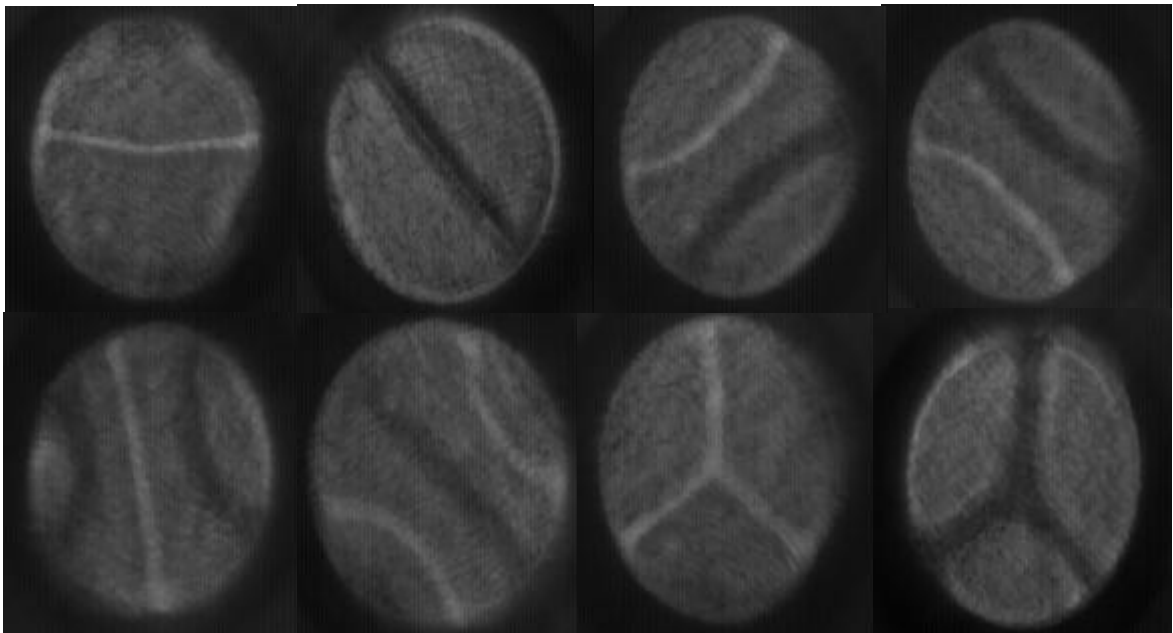


Figure 19. The four basic flow states and their inverted patterns.

The inverted patterns show that there is a simple exchange of white lines (cold falling fluid) for black lines (warm rising fluid) with respect to the original pattern. However the three-roll pattern

in the top right of figure 19 is unique in that the inverted pattern can be made by a simple rotation of the original pattern.

We can calculate the Rayleigh number at which each pattern was found and stabilised from the temperature difference given by the thermocouple. The thermocouple read-out was from a digital voltmeter allowing accuracy in the reading of $\pm 0.003\text{mV}$. We found by slowly increasing the Rayleigh number, that the first signs of a convective flow pattern occurred at $R = 5,300$, and that significant time dependence set in at $R = 25,500$. This is a slight departure from the values in previous works of $R = 3,500$ and $R = 20,000$ respectively [12]. The departure from previous work is also apparent when we calculate the Rayleigh number for “signpost” events in the evolution of a flow state. When lowering the Rayleigh number for a stable two-roll pattern, the onset of instability to the mercedes pattern is described at $R = 10,900$ [12]. When we followed this course we found that the decay to the mercedes flow state consistently occurred at, or around $R = 18,600$, indicating that our operation of the cell was producing similar patterns to previous work, but with an overall rise in Rayleigh number. At this point we could confidently reproduce any one of several flow patterns, and stabilise it almost indefinitely.

4.3 A COMPARISON BETWEEN OPTICAL SYSTEMS

To compare the two optical systems we require images taken with the two-lens system, of the same convective patterns as taken with the four-lens system. This would enable us to determine how the four-lens system will affect the contrast of the image with respect to the images taken with the two-lens system. To enable us to make a valid comparison of the two systems, we created a stable flow pattern in one system, took an image, and swapped to the other system straight away to take another image for comparison with the first. Our initial visual comparison of the images led us to believe that the contrast of the two-lens system was slightly superior to that of the four-lens system. Some of the images we obtained are shown below in figure 20.

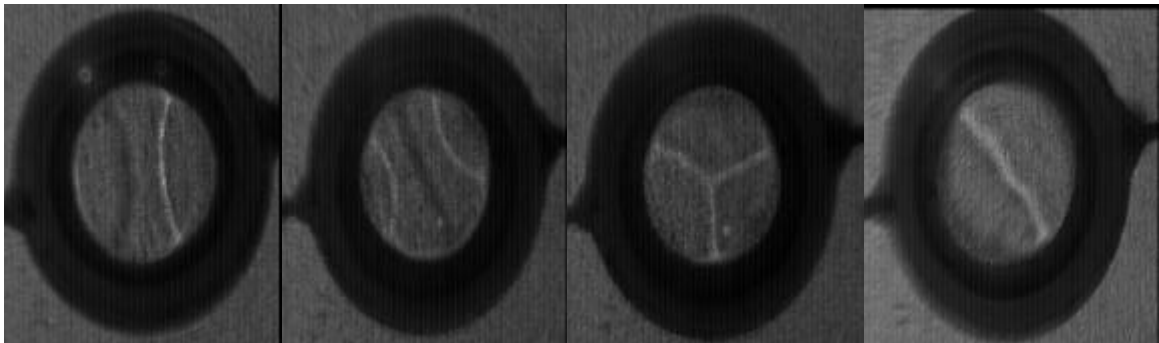


Figure 20. Some of images taken with the two-lens optical system.

The main problem we faced was finding a more scientific method of comparison than simply examining two images with the eye. This was solved by further use of Accuware the software package that we were using to display the images from the CCD camera. Accuware had the capability to perform several types of measurement and mathematical function upon the data enclosed within a user defined region of interest (ROI). One of the measurements that it could do was to read out the maximum and minimum values of intensity across the ROI, as well as averaging the intensity over all the pixels. This meant that a gauge of the contrast could be achieved by calculating a kind of fractional resolution from this information. Therefore that the fractional resolution could be given as C:

$$C = \frac{\Delta I}{I} \quad \text{when} \quad \Delta I = I_{MAX} - I_{MIN}$$

The software limited the size, shape and orientation of the ROI. We were allowed to create the ROI either from a rectangle or a pentagon, although there was no maximum size in either the pentagon or the rectangular case, we were restricted to a minimum width of five pixels for the case of the rectangle. The orientation of the rectangle also caused some problems; we were allowed to position it with the longer side vertically or horizontally, but not at any angle in between. This proved to be very awkward when the flow pattern did not align itself vertically or horizontally, as our ROI would be at some angle to the natural symmetry of the pattern.

There was no way to get round this however so we proceeded by creating a particular flow state in the four-lens system and saving an image of it, then with the pattern stabilised we changed the apparatus over to the two-lens system and again recorded the image of the pattern. This approach allowed us to be sure of imaging the same pattern at comparable Rayleigh numbers for both systems. The job of determining the fractional resolution for each image could be done at a separate time, with the image simply loaded onto the computer screen. Figure 20 shows some of the images taken with the two-lens system for the comparison of fractional resolution with the four-lens system.

The way we used the various ROI was to place three rectangular ROI of minimum width, both horizontally and vertically with one of each group of three placed in the centre of the cell image. The pentagon ROI tool was also used, for this we simply expanded the ROI until we maximised the amount of cell enclosed without including the black cell boundary. In this way we could get a good idea of the variation in intensity across the flow pattern, as well as examining the overall cell intensity with the pentagon ROI.

The intensity of the light incident upon the CCD is converted to an integer value in the range 0-255 to allow for display on the computer screen. However the CCD camera itself has automatic gain control (AGC), and will therefore attempt to keep the maximum or minimum intensity of the image within a certain range. This caused problems when the AGC corrected the intensity of the image to such a degree that it was noticeably brighter than many of our previous images. A comparison between the two images on the right hand side of figure 17 show the problem very clearly, one image having a noticeably higher average intensity. We attempted to combat this by always supplying the same power to the light source, however this caused the two-lens system to “white-out” the camera. This makes sense, the image of the four-lens system will require substantially more light to illuminate its increased area, than the light required in the two-lens case. So we illuminated the four-lens system with the bulb run at 2 Amps, and the two-lens system with the bulb run at 0.4 Amps, these values gave us the same background image intensities.

From the readings we took with the software, it was clear that with the convection in place, the intensity was changed markedly from the images of the non-convecting cell, and that this was a good way of estimating the resolution of the two systems. Tables 6 and 7 show a comparison of the fractional resolution for the two and four-lens systems over a range of flow states.

TABLE 6. COMPARISON OF THE FRACTIONAL RESOLUTION OVER VARIOUS FLOW STATES FOR THE PENTAGON ROI.

ROI type	Two roll	Three roll	Four roll	Mercedes	Inverse two-roll	Inverse four-roll	Inverse four-roll	Error
Pentagon	1.595	1.302	1.259	1.281	1.489	1.179	1.179	±0.022
Pentagon	1.478	1.967	1.686	1.615	1.801	1.614	1.614	±0.010
Difference	-0.117	0.665	0.427	0.334	0.312	0.435	0.435	

TABLE 7. COMPARISON OF THE FRACTIONAL RESOLUTION OVER VARIOUS FLOW STATES FOR STRIP ROI.

ROI type	Two roll	Three roll	Four roll	Mercedes	Inverse two-roll	Inverse four-roll	Inverse four-roll	Error
Strip	1.024	1.058	0.906	0.958	1.057	0.972	0.972	±0.004
Strip	1.041	1.178	1.297	1.117	1.367	1.133	1.133	±0.045
Difference	0.017	0.12	0.391	0.159	0.31	0.161	0.161	

We showed more flow states in figure 19 than are compared in tables 6 and 7, this is due to the instability of some of the states. For instance the inverted mercedes pattern remained stable long enough to record its image with the four lens system but not long enough for us to change to the two-lens system and capture an image.

5. CONCLUSIONS

When looking at the experiment as a whole, several main objectives are apparent; confirmation of images given in previous works, confirmation of the action of the four-lens system to increase the image size, the ability to competently operate both optical systems and the comparison of the contrast of both systems. In conclusion we address each of these in turn, then offer our thoughts on problems that we encountered, and on future work of this type, with particular reference to the equipment we used.

- Confirmation of images given in previous works [12,13].

In this respect we have been particularly successful, we have managed to reproduce the majority of the patterns found previously the only exceptions were the rotating spoke patterns that formed after a large discontinuous jump in Rayleigh number from below R_{crit} . Whilst we did reproduce the images, we did not manage to confirm the ranges of stability or even the Rayleigh numbers at which these patterns were formed, our data not in concordance with that given previously. We discuss this problem further in a later part of these conclusions.

- Confirmation that the four-lens system increases the image size.

We feel justified in saying that the theory given by Croquette [2] has been verified by our experiment. The size of the image in comparison to the overall size of the CCD screen was not what we had intended, it was in fact slightly smaller. However we were working with measurements of the CCD size that have yet to be satisfactorily confirmed and so may be the cause of this slight error. Figure 16 demonstrates the increase in size of the image quite clearly.

- The ability to competently operate both optical systems.

We have demonstrated our ability to set-up both systems, and our choice of switching from one system to the other whilst maintaining a stable flow pattern has shown that we can work both quickly and correctly. Of the two systems, the four-lens was the more difficult to align properly, it may therefore be possible to improve the results for the four-lens system by better optical alignment.

- Comparison of the fractional resolution of the two optical systems.

Unfortunately we have been unable to show that the four-lens system did not degrade the contrast of the image as we had initially hoped, and a small decrease in fractional resolution is observed when making the transition from two to four lenses. However in a comparison of the images in this paper experimentalists may feel that the increase in image size shown in figure 16 will outweigh the loss of fractional resolution that we found. In fact the difference in fractional resolution may be reduced when it is possible to set-up the four-lens system with as much certainty of attaining the best images as can be done with the two-lens system.

Some of the problems that we encountered in the experiment, could have been partly or jointly responsible for the change in contrast between optical systems, they are discussed here. The main problem in the switching over of the systems was ensuring that the same sharpness of image could be maintained from one image with a particular system to then next. In fact examination of tables 4 and 5 shows that in some cases we may have failed in this regard, our main problem was that the optical alignment of the four-lens system involved correctly placing the lens L3 with respect to L2. What made this especially hard, and prone to error, was the distances involved and the physical shape of L3. The position of L3 was only 60mm above that of L2 and the beam we were trying to place in the centre of L3 was approximately 3mm wide compared to the 25mm diameter of L3. When these facts are coupled with the physical shape of L3, which is considerably bowed, we have a link in the chain of good optical alignment that looks extremely error prone.

The other problem that we consistently ran up against was that of the Rayleigh number at which our patterns were being formed and were bifurcating to other patterns; it was always higher than those given by previous works [12,13]. We can only speculate as to the cause of this, however it could be a function of our operation of the apparatus. When the apparatus was last used by Bjorn Hof [12,13], he was able to let the fluid pattern settle before increasing or decreasing the Rayleigh

number further, however time constraints prevented us from such experimental luxuries. What we consider to be a possibility, is that when lowering the Rayleigh number from time dependent values, not stabilising the flow state allows a small measure of time dependence to remain, well below the time dependent threshold. This could well cause the pattern to become unstable to other flow states at a higher Rayleigh number than we would have expected. The time scales over which we were lowering the Rayleigh number were comparable to a few thermal diffusion times, so this is definitely possible. Another possible cause of error is the data we used for the viscosity and the thermal expansion coefficient of the water. These properties change with respect to temperature, we used values for these properties taken in water at 36°C in all instances. However in the range of temperatures over which we operated the cell the change of the value of these “constants” could be up to 100%. The data we used was a good estimation of the true values for temperature differences of greater than 30°C, however it was quite a poor estimation for smaller temperature differences. Calculations with more appropriate data indicate that our values of the Rayleigh number would be significantly more in accordance with those stated in [12,13], as seen in table 8 below.

TABLE 8. COMPARISON OF RECALCULATED RAYLEIGH NUMBERS

Event	Experimental Rayleigh	Recalculated Rayleigh	Rayleigh from [12,13]
First signs of convection	5,300	2,200	3,500
Bifurcation from two-roll to the Mercedes pattern	18,600	12,300	10,900
Onset of significant time dependence	25,500	18,500	20,000

If further work were to be carried out with the apparatus we used we would recommend that a method for better controlling the temperature difference and so the Rayleigh number be found. One very appealing possibility is that of a computer controlled feedback method which could conceivably allow the user to simply enter the required flow state, and the software would then follow the path most likely to produce such a state. Another good improvement would be to modify the mounts for the extra two lenses so that they could more easily be adjusted in the vertical direction. What is currently underway is a wholesale movement of the experiment to an area that will allow for the complete blacking out of any extraneous light, had this not already been thought of it would comprise the third of our recommendations in this section. Any further work in this area would be useful, but an attempt at reproducing some of our flow patterns with another convective cell would be highly instructive. The way is also open for a high precision alignment of the four-lens system to better investigate the contrast of it compared to the usual two-lens system.